Available online at www.sciencedirect.com

ScienceDirect

Applied Mathematical Modelling 01 (2021) 1–29

Applied Mathematical Modelling

Dynamic stiffness method for exact longitudinal free vibration of rods and trusses using simple and advanced theories

Xiang Liu[a,b,c], Yaxing Zhao[a,b,c], Wei Zhou[a,b,c,*], J.Ranjan Banerjee[d]

[a]*Key Laboratory of Traffic Safety on Track, Ministry of Education, School of Traffic & Transportation Engineering, Central South University, Changsha, China*

[b]*Joint International Research Laboratory of Key Technology for Rail Traffic Safety, Central South University, Changsha, China*

[c]*National & Local Joint Engineering Research Center of Safety Technology for Rail Vehicle, Central South University, Changsha, China*

[d]*School of Mathematics, Computer Science and Engineering, City, University of London, London EC1V 0HB, UK*

Abstract

Closed-form dynamic stiffness (DS) formulations coupled with an efficient eigen-solution technique are proposed for exact longitudinal free vibration analyses of rods and trusses by using classical, Rayleigh-Love, Rayleigh-Bishop and Mindlin-Hermann theories. First, the exact general solutions of the governing differential equations of the four rod theories are developed. Then the solutions are substituted into the generalized displacement and force boundary conditions (BCs), leading to the elemental DS matrices utilising symbolic computation. As an accurate and efficient modal solution technique, the Wittrick-Williams (WW) algorithm is applied. The J_0 count for the WW algorithm has been resolved for all four types of DS elements with explicit analytical expressions. The method is verified against some existing exact results for rods subjected to specific BCs. Comparisons of the natural frequencies and mode shapes for different theories and slenderness ratios are also made. Finally, benchmark solutions are provided for individual rods subject to different BCs, a stepped rod and a truss. This research provides an exact and highly efficient modal analysis tool for rods and trusses within the whole frequency range, which is suitable for parametric studies, optimization design, inverse problem analysis, and important for statistical energy analysis.

Keywords: Dynamic stiffness method; Wittrick-Williams algorithm; Rayleigh-Bishop theory; Mindlin-Hermann theory; Broadband dynamics; Modal analysis

1. Introduction

Rods which principally carry tensile and compressive loads are commonly used in engineering. They are widely used as components in piezoelectric applications[1], phononic

*Corresponding author. Tel: +86 (0)13975126342

Email addresses: xiangliu06@gmail.com (Xiang Liu), 1833006046@qq.com (Yaxing Zhao), Zhou_wei000@126.com (Wei Zhou), j.r.banerjee@city.ac.uk (J.Ranjan Banerjee)

crystals[2], damage detection[3] and wave propagation control[4]. Thus the vibration and longitudinal wave propagation analysis of rods are very important in the design of structures.

Many mathematical models describing the longitudinal vibration of rod elements have been proposed. D'Alembert et al.[5] in the 18th century proposed the classical theory of longitudinal vibration analysis based on one-dimensional wave equation, which is suitable for slender members undergoing low frequency vibration. The theory ignored the transverse inertia effect and the corresponding transverse and longitudinal shear modes. Rayleigh[6] considered the importance of transverse inertia effect in his classical book *Theory of Sound* published in 1877. Later, the theory was further developed by Love [7] in 1892. The next generalization of the theory was made by Bishop[8] who modified the Rayleigh-Love theory by taking into account the contribution of the transverse shear effect. The theory is now called the Rayleigh-Bishop theory. From the perspective of engineering application, the Rayleigh-Bishop theory is significantly more complex than the Rayleigh-Love theory, and the predicted resonance frequency is more accurate than the classical theory. Next, Mindlin and Herrmann[9] generalized the Rayleigh–Bishop model by considering the lateral displacement as an independent function of time and space coordinates. Zozulya[10] then made a summary of the high order theory for rods.

The wave propagation and longitudinal vibration of rod elements in structures being very important considerations in engineer applications have drawn significant attentions. Han et al.[11] established the vibration energy flow model of longitudinally vibrating Rayleigh–Love and Rayleigh–Bishop rods. They also compared the energy flow analysis results with analytical solutions. Machado and Santos[12] analysed the effect of parametric distributed uncertainties in longitudinal wave propagation of Rayleigh-Love rod using spectral element method. Krawczuk et al.[13, 14] introduced the Rayleigh-Love theory for the lower excitation frequency, and the Mindlin-Herrmann models for higher frequency excitation. Mei[15]analysed the dynamics of longitudinal vibration of rods from the point of view of wave motion. Yang[16] presented a unified analytical solution to the wave equation which controls the propagation of longitudinal stress waves in elastic rods. Fedotov et al.[17–19] analysed the vibration of a Rayleigh-Bishop rod under different conditions in terms of a Green function. Tenkam et al.[20] gave the analytical solution in terms of Green's functions of the Mindlin–Herrmann model for longitudinal vibration of an isotropic rod with constant cross-section. Güven[21] investigated the propagation of the longitudinal stress waves of Rayleigh–Bishop and Mindlin–Herrmann rods using the modified couple stress theory. Żak and Krawczuk[22] highlighted some of the major differences and similarities between different rod theories and discussed certain numerical aspects of their applications. Wang et al.[23–25] analysed the free vibration and wave propagation of beams and plates using Rayleigh-Ritz method. Shen et al.[26] modelled the dispersive waves in cracked rods based on higher-order rod theories using wavelet finite element method. Gan et al.[27] established their formulation based on Mindlin-Herrmann theory. The propagation characteristics of the longitudinal wave in variable cross section rods were studied by them by using the transfer matrix method. Lim et al.[28, 29] developed different methods for the analysis of free vibration of beams. Chen et al.[30, 31] analyzed the transverse vibration of longitudinally moving beams considering finite deformation together with viscoelastic foundation using a complex modal analysis

method. Zhang et al.[32] investigated the dynamic stability of longitudinally transporting viscoelastic beams with two-frequency parametric excitation using the perturbation technique. Yan et al.[33] studied the dynamics of a Mindlin–Herrmann rod with surface piezoelectric patches adopting the reverberation matrix method. Sun et al.[34] proposed the generalized finite difference method to solve space-fractional diffusion equations. Cao et al.[35–37] analysed the vibrations of rods with the help of the Cosserat rod element approach. Dai and Xiao[38] studied a new deployable truss structure using the Moore–Penrose generalized inverse matrix method. Nevertheless, most of the above methods for modelling the longitudinal vibration of rods have the following limitations. (i) Different formulae are needed for different boundary conditions, (ii) Analytical solutions are only for indvidual elements, thus not capable of modelling built-up structures, especially when the longitudinal and bending vibration are coupled, (iii) Eigensolution techniques such as matrix determinant are not efficient and reliable, and thus sometimes the methods can miss some of the eigen-roots.

Different from the above methods, the dynamic stiffness method (DSM)[39] is an exact analytical method which can be applied to built-up structures subjected to any boundary conditions and has an efficient and reliable eigenvalue and response algorithm. Many researchers have developed dynamic stiffness models in the frequency domain for beams[40–44], membranes[45, 46], plates[47–49], shell[50, 51], multi-layered half-space[52], amongst others. Moreover, DSM can be applied to many other related problems, such as the dynamic response[53–55], wave propagation[56], energy flow analysis[57] and so on. For example, Ding et al.[58] established dynamic stiffness models for free vibration of an longitudinally moving beam with both ends supported by torsional springs and vertical springs. Wu[57] applied the dynamic stiffness method to the energy flow analysis of plate built-up structures. Bercin[59] used dynamic stiffness method as a benchmark to check the effectiveness of statistical energy analysis and wave intensity method. Chen et al.[53, 54] conducted the response analysis of longitudinally loaded beam on a viscoelastic foundation using the dynamic stiffness method based on Timoshenko theory. Ba et al.[60] studied the 3D dynamic responses of a multi-layered half-space subjected to concentrated forces and pore pressure with the aid of dynamic stiffness matrix. Doyle[56] analysed the wave propagation in structures using the spectral analysis method. For modal analysis, the Wittrick-Williams algorithm[61, 62] is an effective way to extract eigenvalues from the transcendental dynamic stiffness matrix. With the help of Wittrick-Williams algorithm, the degrees of freedom needed to model the structures can be very few, but nevertheless, exact natural frequencies can be computed.

Therefore, the main purpose of this paper is to develop exact dynamic stiffness formulations using four different rod theories, namely the classical, Rayleigh–Love, Rayleigh-Bishop and Mindlin-Herrmann theories. The associated mode count technique for the eigenvalue solution technique using Wittrick-Williams algorithm is significantly enhanced. The method is then used to investigate the longitudinal free vibration behaviour of rods. The paper is organized as follows. Following this Introduction, Section 2 develops the dynamic stiffness matrices of the rod based on the above four different rod theories, and the explicit form of the element of dynamic stiffness matrices are derived. Then, Section 3 fomulates the J_0 count in the W-W algorithm, followed by the computation procedure of mode shapes. Section 4 demonstrates the high accuracy and efficiency of the dynamic

stiffness method by comparing the results with some published results for natural frequencies using various rod theories for different boundary conditions. Furthermore, the applications of dynamic stiffness method in vibration analysis of a stepped rod and a pin-jointed plane frame are demostrated. Finally, Section 5 concludes the paper.

2. Dynamic stiffness formulations for free longitudinal vibration based on different rod theories

This section develops the dynamic stiffness (DS) formulations for a rod element based on four different theories. It should be noted that the solutions of classical (Section 2.1) and Rayleigh-Love theories (Section 2.2) can be found in the literature[63], which is given here for the sake of completeness and also to make the paper self-contained. But the dynamic stiffness (DS) formulations for the Rayleigh-Bishop (Section 2.3) and Mindlin-Herrmann theories (Section 2.4) are new and proposed for the first time.

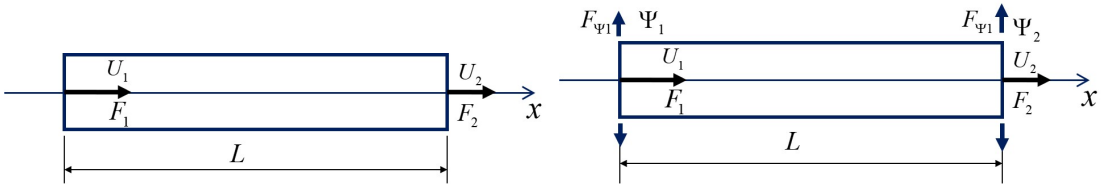

(a) Classical and Rayleigh-Love theories (b) Rayleigh-Bishop and Mindlin-Herrmann theories

Fig. 1. The generalised displacement and force boundry conditions of rod elements based on the classical and Rayleigh-Love theories(a), the Rayleigh-Bishop and Mindlin-Herrmann theories(b).

2.1. DS formulation for the classical theory

A rod model based on the classical (C) theory is shown in Fig.1(a). The element has length L with constant cross section A. The classical theory assumes that the longitudinal deformations along the neutral axis of the rod are the same at all points on the cross section and that the transverse deflections are negligible. By using Hamilton's principle, the governing differential equation (GDE) in the time domain for a rod based on the classical theory can be deduced as follows[64]

$$EA\frac{\partial^2 u}{\partial x^2} - \rho A\frac{\partial^2 u}{\partial t^2} = 0 \tag{1}$$

where EA is the longitudinal stiffness of the rod, ρ is the density of the material, A is the cross-sectional area of the rod, $u(x,t)$ is the longitudinal displacement of the rod cross section at distance x from the origin and t is time. It can be shown from natural boundary conditions that the expression for the longitudinal force $f(x,t)$ is given by

$$f(x,t) = EA\frac{\partial u}{\partial x} \tag{2}$$

Assuming that the rod longitudinal vibration is a simple harmonic vibration with an angular frequency of ω, one can be write

$$u(x,t) = U(x)\sin(\omega t) \tag{3}$$

where $U(x)$ is the amplitude of longitudinal vibration. Substituting Eq.(3) into Eq.(1), we have

$$U''(x) + \frac{\omega^2}{a^2}U(x) = 0 \tag{4}$$

where $a = \sqrt{E/\rho}$. This equation is a second-order ordinary differential equation of U in terms of x, and its solution can be obtained as

$$U(x) = C_1 \cos\left(\frac{\omega}{a}x\right) + C_2 \sin\left(\frac{\omega}{a}x\right) \tag{5}$$

where C_1 and C_2 are constants. Substituting Eq.(5) into Eq.(2), the expression for the amplitude of the longitudinal force becomes

$$F(x) = EA\frac{\mathrm{d}U}{\mathrm{d}x} \tag{6}$$

Now referring to Fig.1(a), the boundary conditions for displacements and forces at both ends of the rod can be applied as follows.

$$U(0) = U_1, F(0) = -F_1, (x = 0) \tag{7a}$$

$$U(L) = U_2, F(L) = F_2, (x = L) \tag{7b}$$

Substituting Eq.(7) into Eqs.(5) and (6), the following matrix relations can be obtained as

$$\begin{bmatrix} U_1 \\ U_2 \end{bmatrix} = \begin{bmatrix} 1 & 0 \\ \cos\alpha & \sin\alpha \end{bmatrix} \begin{bmatrix} C_1 \\ C_2 \end{bmatrix} \tag{8}$$

$$\begin{bmatrix} F_1 \\ F_2 \end{bmatrix} = EA \begin{bmatrix} 0 & -\frac{\omega}{a} \\ -\frac{\omega}{a}\sin\alpha & \frac{\omega}{a}\cos\alpha \end{bmatrix} \begin{bmatrix} C_1 \\ C_2 \end{bmatrix} \tag{9}$$

where $\alpha = \omega L/a$.

By eliminating the constants C_1 and C_2 in Eqs.(8) and (9), the dynamic stiffness formula for longitudinal vibration of a beam can be obtained, namely

$$\begin{bmatrix} F_1 \\ F_2 \end{bmatrix} = \frac{EA\alpha}{L} \begin{bmatrix} \cot\alpha & -\csc\alpha \\ -\csc\alpha & \cot\alpha \end{bmatrix} \begin{bmatrix} U_1 \\ U_2 \end{bmatrix} \tag{10}$$

Eq.(10) can also be written as follows

$$\boldsymbol{f} = \boldsymbol{K}_C \boldsymbol{d} \tag{11}$$

where $\boldsymbol{f} = \begin{bmatrix} F_1 & F_2 \end{bmatrix}^T$ represents the column vector of the force at both ends, $\boldsymbol{d} = \begin{bmatrix} U_1 & U_2 \end{bmatrix}^T$ represents the displacement column vector at both ends. $\boldsymbol{K}_C$ represents the dynamic stiffness matrix for the longitudinal vibration of the rod element based on the classical theory in the local coordinate system, namely

$$\boldsymbol{K}_C = \frac{EA\alpha}{L} \begin{bmatrix} \cot\alpha & -\csc\alpha \\ -\csc\alpha & \cot\alpha \end{bmatrix} \tag{12}$$

2.2. DS formulation for the Rayleigh-Love theory

A rod model based on the Rayleigh-Love (R-L) theory is shown in Fig.1(a). The R-L theory is the simplest generalization of the classical model by including the effects of the

lateral motion. The governing differential equation (GDE) in the time domain for a rod based on the R-L theory can be expressed in the following form[64]

$$EA\frac{\partial^2 u}{\partial x^2} + \nu^2 \rho I_p \frac{\partial^4 u}{\partial x^2 \partial t^2} - \rho A \frac{\partial^2 u}{\partial t^2} = 0 \tag{13}$$

where ν is the Poisson ratio of the material, I_p is the polar moment of inertia, $u(x,t)$ is the longitudinal displacement of the rod cross section from the origin x at time t. It can be obtained from natural boundary conditions that the expression for the longitudinal force $f(x,t)$ is as follow

$$f(x,t) = EA\frac{\partial u}{\partial x} + \nu^2 \rho I_p \frac{\partial^3 u}{\partial x \partial t^2} \tag{14}$$

If harmonic oscillation is assumed, then

$$u(x,t) = U(x)\sin(\omega t) \tag{15}$$

where ω is the angular frequency, and $U(x)$ is the amplitudes of u. Substituting Eq.(15) into Eq.(13) gives

$$\left(EA - \rho I_p \nu^2 \omega^2\right)\frac{\mathrm{d}^2 U}{\mathrm{d}x^2} + \rho A \omega^2 U = 0 \tag{16}$$

This equation is a second-order ordinary differential equation of U in terms of x, whose solution can be obtained as

$$U(x) = C_1 \cos\left(\frac{\omega}{a}x\right) + C_2 \sin\left(\frac{\omega}{a}x\right) \tag{17}$$

where $a = \sqrt{\frac{EA - \nu^2 \rho I_p \omega^2}{\rho A}}$, and C_1 and C_2 are arbitrary constants. Substituting Eq.(15) into Eq.(14), the expression for the amplitude of the longitudinal force becomes

$$F(x) = (EA - \rho I_p \nu^2 \omega^2)\frac{\mathrm{d}U}{\mathrm{d}x} \tag{18}$$

Now referring to Fig.1(a), the boundary conditions for displacements and forces at both ends of the rod can be applied as follows

$$U(0) = U_1, F(0) = -F_1, (x = 0) \tag{19a}$$

$$U(L) = U_2, F(L) = F_2, (x = L) \tag{19b}$$

Substituting Eq.(19) into Eqs.(17) and (18), the relationships between displacement vector and constant vector, force vector and constant vector can be derived respectively.

$$\begin{bmatrix} U_1 \\ U_2 \end{bmatrix} = \begin{bmatrix} 1 & 0 \\ \cos\alpha & \sin\alpha \end{bmatrix} \begin{bmatrix} C_1 \\ C_2 \end{bmatrix} \tag{20}$$

$$\begin{bmatrix} F_1 \\ F_2 \end{bmatrix} = \frac{(EA - \rho I_p \nu^2 \omega^2)\,\alpha}{L} \begin{bmatrix} 0 & -1 \\ -\sin\alpha & \cos\alpha \end{bmatrix} \begin{bmatrix} C_1 \\ C_2 \end{bmatrix} \tag{21}$$

where $\alpha = \omega L/a$.

The DS formulation can be obtained by eliminating the coefficients C_1 and C_2 from Eqs.(20) and (21) and is given by

$$\begin{bmatrix} F_1 \\ F_2 \end{bmatrix} = \frac{\alpha\,(EA - \rho I_p \nu^2 \omega^2)}{L} \begin{bmatrix} \cot\alpha & -\csc\alpha \\ -\csc\alpha & \cot\alpha \end{bmatrix} \begin{bmatrix} U_1 \\ U_2 \end{bmatrix} \tag{22}$$

Eq.(22) can also be written as follows

$$\boldsymbol{f} = \boldsymbol{K}_{RL}\boldsymbol{d} \tag{23}$$

where $\boldsymbol{f} = \begin{bmatrix} F_1 & F_2 \end{bmatrix}^T$ represents the column vector of the force at both ends of the rod element, $\boldsymbol{d} = \begin{bmatrix} U_1 & U_2 \end{bmatrix}^T$ represents the displacement column vector at both ends. $\boldsymbol{K}_{RL}$ represents the dynamic stiffness matrix for the longitudinal vibration of the rod element based on the R-L theory in the local coordinate system, namely

$$\boldsymbol{K}_{RL} = \frac{\alpha\left(EA - \rho I_p \nu^2 \omega^2\right)}{L}\begin{bmatrix} \cot\alpha & -\csc\alpha \\ -\csc\alpha & \cot\alpha \end{bmatrix} \tag{24}$$

2.3. DS formulation for the Rayleigh-Bishop theory

The governing differential equation (GDE) in the time domain for a rod based on the Rayleigh-Bishop(R-B) theory can be expressed in the following form[64]

$$\nu^2 G I_p \frac{\partial^4 u}{\partial x^4} - \nu^2 \rho I_p \frac{\partial^4 u}{\partial x^2 \partial t^2} - EA\frac{\partial^2 u}{\partial x^2} + \rho A \frac{\partial^2 u}{\partial t^2} = 0 \tag{25}$$

where E is the Young's modulus of the material, $G = \frac{E}{2(1+\nu)}$ is the shear modulus, $u(x,t)$ is the longitudinal displacement of the rod cross section from the origin x at time t. It can be obtained from natural boundary conditions that the expression for the longitudinal force $f(x,t)$ is as follow

$$f(x,t) = EA\frac{\partial u}{\partial x} + \nu^2 \rho I_p \frac{\partial^3 u}{\partial x \partial t^2} - \nu^2 G I_p \frac{\partial^3 u}{\partial x^3} \tag{26}$$

Assuming that the longitudinal vibration is a simple harmonic vibration with an angular frequency of ω over time t, that is

$$u(x,t) = U(x)\sin(\omega t) \tag{27}$$

where ω is the angular frequency, and $U(x)$ is the amplitudes of u. Substituting Eq.(27) into Eq.(25) gives

$$\nu^2 G I_p \frac{\mathrm{d}^4 U}{\mathrm{d}x^4} + (\rho\nu^2 I_p \omega^2 - EA)\frac{\mathrm{d}^2 U}{\mathrm{d}x^2} - \rho A \omega^2 U = 0 \tag{28}$$

Obviously, Eq.(28) is a fourth-order ordinary differential equation with the longitudinal vibration amplitude $U(x)$, and its characteristic equation is

$$r^4 + \frac{(\rho\nu^2 I_p\omega^2 - EA)}{G\nu^2 I_p} r^2 - \frac{\rho A \omega^2}{G\nu^2 I_p} = 0 \tag{29}$$

The solution of Eq.(29) is given by $r_{1,2} = \pm i\alpha$, $r_{3,4} = \pm\beta$, where i is the imaginary unit and

$$\begin{aligned} \alpha &= \sqrt{\frac{(\rho\nu^2 I_p\omega^2 - EA) + \sqrt{(\rho\nu^2 I_p\omega^2 - EA)^2 + 4\rho A G\nu^2 I_p\omega^2}}{2G\nu^2 I_p}} \\ \beta &= \sqrt{\frac{-(\rho\nu^2 I_p\omega^2 - EA) + \sqrt{(\rho\nu^2 I_p\omega^2 - EA)^2 + 4\rho A G\nu^2 I_p\omega^2}}{2G\nu^2 I_p}} \end{aligned} \tag{30}$$

The solution of Eq.(28) is given by

$$U(x) = C_1 \sin \alpha x + C_2 \cos \alpha x + C_3 \sinh \beta x + C_4 \cosh \beta x \tag{31}$$

The lateral deformation is

$$\Psi(x) = C_1 \alpha \cos \alpha x - C_2 \alpha \sin \alpha x + C_3 \beta \cosh \beta x + C_4 \beta \sinh \beta x \tag{32}$$

where C_1, C_2, C_3 and C_4 are constants. Substituting Eq.(27) into Eq.(26), the expression for the amplitude of the force can be given by

$$F_u = (EA - \rho I_p \nu^2 \omega^2) \frac{\mathrm{d}U}{\mathrm{d}x} - \nu^2 G I_p \frac{\mathrm{d}^3 U}{\mathrm{d}x^3} \tag{33a}$$

$$F_\psi = \nu^2 G I_p \frac{\mathrm{d}^2 U}{\mathrm{d}x^2} \tag{33b}$$

Now referring to Fig.1(b), the boundary conditions for displacements and forces at both ends of the rod can be applied as follows.

$$U(0) = U_1, \Psi(0) = \Psi_1, F_u(0) = -F_{u1}, F_\psi(0) = -F_{\psi 1} \tag{34a}$$

$$U(L) = U_2, \Psi(L) = \Psi_2, F_u(L) = F_{u2}, F_\psi(L) = F_{\psi 2} \tag{34b}$$

Substituting Eq.(34) into Eqs.(31), (32) and (33), the relationships between displacement and constant vectors, between force and constant vectors can be derived respectively.

$$\begin{bmatrix} U_1 \\ \Psi_1 \\ U_2 \\ \Psi_2 \end{bmatrix} = \begin{bmatrix} 0 & 1 & 0 & 1 \\ \alpha & 0 & \beta & 0 \\ \mathrm{s} & \mathrm{c} & S & C \\ \alpha\,\mathrm{c} & -\alpha\,\mathrm{s} & \beta C & \beta S \end{bmatrix} \begin{bmatrix} C_1 \\ C_2 \\ C_3 \\ C_4 \end{bmatrix} \tag{35}$$

$$\begin{bmatrix} F_{u1} \\ F_{\psi 1} \\ F_{u2} \\ F_{\psi 2} \end{bmatrix} = \begin{bmatrix} \alpha\left(EA - \rho I_p \nu^2 \omega^2\right) + \nu^2 G I_p \alpha^3 & 0 \\ 0 & -\alpha^2 \nu^2 G I_p \\ -\left[\left(EA - \rho I_p \nu^2 \omega^2\right)\alpha + \nu^2 G I_p \alpha^3\right] c & \left[\left(EA - \rho I_p \nu^2 \omega^2\right)\alpha + \nu^2 G I_p \alpha^3\right] s \\ \nu^2 G I_p \alpha^2 s & \nu^2 G I_p \alpha^2 c \\ \left(EA - \rho I_p \nu^2 \omega^2\right)\beta - \nu^2 G I_p \beta^3 & 0 \\ 0 & \beta^2 \nu^2 G I_p \\ -\left[\left(EA - \rho I_p \nu^2 \omega^2\right)\beta - \nu^2 G I_p \beta^3\right] C & -\left[\left(EA - \rho I_p \nu^2 \omega^2\right)\beta - \nu^2 G I_p \beta^3\right] S \\ \nu^2 G I_p \beta^2 S & \nu^2 G I_p \beta^2 C \end{bmatrix} \begin{bmatrix} C_1 \\ C_2 \\ C_3 \\ C_4 \end{bmatrix} \tag{36}$$

where $c = \cos(\alpha L), s = \sin(\alpha L), C = \cosh(\beta L)$ and $S = \sinh(\beta L)$.

By eliminating the constant vector from Eqs.(35) and (36), the dynamic stiffness formulation for the Rayleigh-Bishop theory can be written as

$$\boldsymbol{f} = \boldsymbol{K}_{RB} \boldsymbol{d} \tag{37}$$

where $\boldsymbol{f} = \begin{bmatrix} F_{u1} & F_{\psi 1} & F_{u2} & F_{\psi 2} \end{bmatrix}^T$ represents the column vector of the force at both ends, $\boldsymbol{d} = \begin{bmatrix} U_1 & \Psi_1 & U_2 & \Psi_2 \end{bmatrix}^T$ represents the displacement column vector at both ends, $\boldsymbol{K}_{RB}$ represents the dynamic stiffness matrix for the R-B theory in the local coordinate system,

namely

$$\boldsymbol{K}_{RB} = \begin{bmatrix} G_1 & G_2 & G_4 & G_5 \\ G_2 & G_3 & -G_5 & G_6 \\ G_4 & -G_5 & G_1 & -G_2 \\ G_5 & G_6 & -G_2 & G_3 \end{bmatrix} \tag{38}$$

where

$$\begin{aligned} G_1 &= -b\Gamma\left(\alpha Cs + \beta Sc\right)/\delta \\ G_2 &= -b(p - cCp + 2bsS)/\delta \\ G_3 &= \Gamma\left(\alpha Cs - \beta Sc\right)/\delta \\ G_4 &= b\Gamma\left(\alpha s + \beta S\right)/\delta \\ G_5 &= b\left(c - C\right)/\delta \\ G_6 &= 2\Gamma\left(-\alpha S + \beta s\right)/\delta \\ \delta &= [b(1 - cC) - psS/2]/(G\nu^2 I_p) \\ b &= \alpha\beta, 2\Gamma = \alpha^2 + \beta^2, p = \alpha^2 - \beta^2 \end{aligned} \tag{39}$$

2.4. DS formulation for the Mindlin-Herrmann theory

A cylindrical rod model based on the Mindlin-Herrmann theory is shown in Fig.1(b). (The DS formulation for a Mindlin-Herrmann rod with rectangular section is given in the Appendix). The Mindlin–Herrmann theory can be developed taking into account the lateral displacements and by considering the Poisson effect between longitudinal and transverse deformations and it assumes uniform distribution of the longitudinal displacement in the cross-section of the rod. The governing differential equation (GDE) in the time domain for a cylindrical rod based on the Mindlin-Herrmann theory can be expressed in the following form[65]

$$(2\mu + \lambda)A\frac{\partial^2 u}{\partial x^2} + 2\lambda A\frac{\partial \psi}{\partial x} = \rho A\frac{\partial^2 u}{\partial t^2} \tag{40}$$

$$\mu I_p\frac{\partial^2 \psi}{\partial x^2} - 4(\mu + \lambda)A\psi - 2\lambda A\frac{\partial u}{\partial x} = \rho I_p\frac{\partial^2 \psi}{\partial t^2} \tag{41}$$

where $\mu = E/[2(1+\nu)], \lambda = \nu E/[(1+\nu)(1-2\nu)]$ are the Lamé coefficient, $u(x,t)$ is the longitudinal displacement of the rod cross section from the origin x at time t. The natural boundary conditions are as follows

$$f_u = (\lambda + 2\mu)\, A\frac{\partial u}{\partial x} + 2\lambda A\psi \tag{42a}$$

$$f_\psi = \mu I_p\frac{\partial \psi}{\partial x} \tag{42b}$$

Assuming that both the lateral and the longitudinal displacements undergo a simple harmonic vibration with an angular frequency of ω over time t, that is

$$u(x,t) = U(x)\sin(\omega t) \tag{43a}$$

$$\psi(x,t) = \Psi(x)\sin(\omega t) \tag{43b}$$

where $U(x)$ and $\Psi\left(x\right)$ are the amplitudes of longitudinal and lateral vibrations, respectively. Substituting Eq.(43) into Eqs.(40) and (41) gives

$$\begin{bmatrix} (2\mu + \lambda)Ak^2 + \rho A\omega^2 & 2\lambda Ak \\ 2\lambda Ak & -\mu I_p k^2 + 4(\mu + \lambda)A - \rho I_p\omega^2 \end{bmatrix} \begin{bmatrix} U \\ \Psi \end{bmatrix} = \begin{bmatrix} 0 \\ 0 \end{bmatrix} \tag{44}$$

where $k = \frac{\mathrm{d}}{\mathrm{dx}}$. Setting the determinant of the coefficient matrix of Eq.(44) equal to zero gives the characteristic equation as

$$a_2 k^4 - a_1 k^2 + a_0 = 0 \tag{45}$$

where

$$\begin{aligned} a_2 &= (2\mu + \lambda) A \mu I_p, \\ a_1 &= (2\mu + \lambda) A \rho I_p \omega^2 + \rho A \omega^2 \mu I_p - 4\mu(2\mu + 3\lambda) A^2, \\ a_0 &= -\rho A \omega^2 [4(\mu + \lambda) A - \rho I_p \omega^2] \end{aligned}$$

The solution of Eq.(45) is given by

$$k_i^2 = \frac{a_1 \pm \sqrt{a_1^2 - 4 a_2 a_0}}{2 a_2} \tag{46}$$

when $i = 1$, take '+'; when $i = 2$, take '-'. Then the general solution of the rod displacement is

$$U(x) = A_1 R_1 \sinh k_1 x + A_2 R_1 \cosh k_1 x + A_3 R_2 \sinh k_2 x + A_4 R_2 \cosh k_2 x \tag{47a}$$

$$\Psi(x) = A_1 \cosh k_1 x + A_2 \sinh k_1 x + A_3 \cosh k_2 x + A_4 \sinh k_2 x \tag{47b}$$

where $R_i = \frac{-2k_i \lambda A}{(2\mu+\lambda) A k_i^2 + \rho A \omega^2} = \frac{-2k_i \lambda}{(2\mu+\lambda) k_i^2 + \rho \omega^2}, i = 1, 2$. Substituting Eq.(43) into Eq.(42), the expression for the amplitude of the force can be given by

$$F_u = (\lambda + 2\mu) A \frac{\mathrm{d}U}{\mathrm{d}x} + 2\lambda A \Psi \tag{48a}$$

$$F_\psi = \mu I_p \frac{\mathrm{d}\Psi}{\mathrm{d}x} \tag{48b}$$

Now referring to Fig.1(b), the boundary conditions for displacements and forces at both ends of the rod can be applied as follows

$$U(0) = U_1, \Psi(0) = \Psi_1, F_u(0) = -F_{u1}, F_\psi(0) = -F_{\psi 1} \tag{49a}$$

$$U(L) = U_2, \Psi(L) = \Psi_2, F_u(L) = F_{u2}, F_\psi(L) = F_{\psi 2} \tag{49b}$$

Substituting Eq.(49) into Eqs.(47) and (48), the relationships between displacement and constant vectors, force and constant vectors can be derived respectively.

$$\begin{bmatrix} U_1 \\ \Psi_1 \\ U_2 \\ \Psi_2 \end{bmatrix} = \begin{bmatrix} 0 & R_1 & 0 & R_2 \\ 1 & 0 & 1 & 0 \\ R_1 Sh_1 & R_1 Ch_1 & R_2 Sh_2 & R_2 Ch_2 \\ Ch_1 & Sh_1 & Ch_2 & Sh_2 \end{bmatrix} \begin{bmatrix} C_1 \\ C_2 \\ C_3 \\ C_4 \end{bmatrix} \tag{50}$$

$$\begin{bmatrix} F_{u1} \\ F_{\psi 1} \\ F_{u2} \\ F_{\psi 2} \end{bmatrix} = \begin{bmatrix} -k_1 M_1 R_1 - 2M_2 & 0 & (-k_2 M_1 R_2 - 2M_2) & 0 \\ 0 & -k_1 M_3 & 0 & -k_2 M_3 \\ (k_1 M_1 R_1 + 2M_2) Ch_1 & (k_1 M_1 R_1 + 2M_2) Sh_1 & (k_2 M_1 R_2 + 2M_2) Ch_2 & (k_2 M_1 R_2 + 2M_2) Sh_2 \\ k_1 M_3 Sh_1 & k_1 M_3 Ch_1 & k_2 M_3 Sh_2 & k_2 M_3 Ch_2 \end{bmatrix} \begin{bmatrix} C_1 \\ C_2 \\ C_3 \\ C_4 \end{bmatrix} \tag{51}$$

where $Ch_1 = \cosh(Lk_1), Sh_1 = \sinh(Lk_1), Ch_2 = \cosh(Lk_2), Sh_2 = \sinh(Lk_2)$ and $M_1 = (2\mu + \lambda) A, M_2 = \lambda A, M_3 = \mu I_p$.

By eliminating the constant vector from Eqs.(50) and (51), the DS formulation for the

Mindlin-Herrmann theory can be derived as

$$\boldsymbol{f} = \boldsymbol{K}_{MH}\boldsymbol{d} \tag{52}$$

where $\boldsymbol{f} = \begin{bmatrix} F_{u1} & F_{\psi 1} & F_{u2} & F_{\psi 2} \end{bmatrix}^T$ represents the force vector, $\boldsymbol{d} = \begin{bmatrix} U_1 & \Psi_1 & U_2 & \Psi_2 \end{bmatrix}^T$ represents the displacement vector at both ends, $\boldsymbol{K}_{MH}$ represents the DS matrix of the Mindlin-Herrmann theory in the local coordinate system, namely

$$\boldsymbol{K}_{MH} = \begin{bmatrix} G_1 & G_2 & G_4 & G_5 \\ G_2 & G_3 & -G_5 & G_6 \\ G_4 & -G_5 & G_1 & -G_2 \\ G_5 & G_6 & -G_2 & G_3 \end{bmatrix} \tag{53}$$

where

$$\begin{aligned}
G_1 &= M_1\left(-R_2Ch_2Sh_1 + R_1Ch_1Sh_2\right)\left(R_1k_1 - R_2k_2\right)/\delta \\
G_2 &= M_3\left[R_1\left(-Sh_1Sh_2k_1 - k_2 + Ch_1Ch_2k_2\right) + R_2\left(-k_1 + Ch_1Ch_2k_2 - Sh_1Sh_2k_2\right)\right]/\delta \\
G_3 &= M_3\left(-R_1Ch_2Sh_1 + R_2Ch_1Sh_2\right)\left(R_2k_1 - R_1k_2\right)/\delta \\
G_4 &= -M_1\left(-R_2Sh_1 + R_1Sh_2\right)\left(R_1k_1 - R_2k_2\right)/\delta \\
G_5 &= M_3\left(Ch_1 - Ch_2\right)\left(R_2k_1 - R_1k_2\right)/\delta \\
G_6 &= -M_3\left(-R_1Sh_1 + R_2Sh_2\right)\left(R_2k_1 - R_1k_2\right)/\delta \\
\delta &= 2R_1R_2\left(1 - Ch_1Ch_2\right) + \left(R_1^2 + R_2^2\right)Sh_1Sh_2
\end{aligned} \tag{54}$$

3. The Wittrick-Williams algorithm and mode shape computation

Unlike the numerical matrices commonly used in the finite element method, the elements of the dynamic stiffness matrix here are transcendental functions of the frequencies. Therefore, linear algebraic solvers for numerical eigenvalue problems cannot be applied to extract the eigensolutions from the dynamic stiffness formulation. In this respect, the Wittrick-Williams algorithm is a reliable and accurate method for the free vibration analysis based on the dynamic stiffness formulation. The Wittrick-Williams algorithm stems from the Rayleigh theorem, combined with the properties of the Sturm sequence. The natural frequency can be converged upon by the bisection method or similar method up to any required accuracy. In the Wittrick-Williams algorithm, Eq.(55) is used to calculate the mode count J when the circular frequency ω is lower than ω^*.

$$J = \sum_{i}^{m} J_{0i}(\omega^*) + s\left(\boldsymbol{K}(\omega^*)\right) \tag{55}$$

where ω^* is a given trial frequency ($\omega^* \geq 0$); $s\left(\boldsymbol{K}(\omega^*)\right)$ is the number of negative diagonal elements after upper triangular transformation by performing Gauss elimination of $\boldsymbol{K}(\omega)$ evaluated at $\omega = \omega^*$. $J_{0i}(\omega^*)$ is the number of natural frequencies between $\omega = 0$ and $\omega = \omega^*$ for an individual element when both ends of the element are fully clamped. m is the total number of elements composing the structure. The calculating of J_{0i} is crucial in the Wittrick-Williams algorithm, whose solutions will be provided as follows. It should be noted that the solutions of classical theory and Rayleigh-Love theory (Section 3.1) can be found in the literature[63], but those for the Rayleigh-Bishop and Mindlin-Herrmann theories (Section 3.2 and Section 3.3) are proposed for the first time, according to the best knowledge of the authors.

3.1. The J_0 count for the classical theory and Rayleigh-Love theory

For the classical theory and Rayleigh- Love theory, when both ends of the rod element are fixed, combining the physical meaning of the dynamic stiffness, it is known that all elements in the dynamic stiffness matrix of the rod element should have infinite number of natural frequencies, i.e.

$$\sin\alpha = \sin\left(n\pi\right) = 0 \tag{56}$$

Then J_0 can be easily obtained, given by[63]

$$J_0\left(\omega\right) = \text{floor}\left(\frac{\omega L}{a\pi}\right) \tag{57}$$

where $a = \sqrt{E/\rho}$ for the classical theory, $a = \sqrt{(EA - \nu^2\rho I_p\omega^2)/(\rho A)}$ for the Rayleigh-Love theory and floor($\bullet$) is the floor function representing the largest integer number not smaller than $'\bullet'$.

3.2. The J_0 count for the Rayleigh-Bishop theory

For Rayleigh-Bishop theory, it is difficult to determine the frequency number J_0 of fixed supports at both ends directly, but it is easy to find the mode count J_s of the element with both ends simply supported. According to Wittrick-Williams algorithm, J_s can be given by,

$$J_s = J_0 + s(\boldsymbol{B}) \tag{58}$$

in which $\boldsymbol{B}$ is the dynamic stiffness matrix for the rod element with both ends simply supported, i.e., $\boldsymbol{B} = \begin{bmatrix} G_3 & G_6 \\ G_6 & G_3 \end{bmatrix}$. Thus the expression of J_0 for Rayleigh-Bishop theory can be given by

$$J_0 = J_s - s(\boldsymbol{B}) \tag{59}$$

For a Rayleigh-Bishop rod simply supported on both ends, we have

$$U\left(0\right) = U\left(L\right) = F_\psi\left(0\right) = F_\psi\left(L\right) = 0 \tag{60}$$

We can assume

$$U\left(x\right) = \sin\left(\frac{m\pi}{L}x\right) \tag{61}$$

where $m = 0, 1, 2, 3...$ Substituting Eq.(61) into Eq.(25), we can get a fourth polynomial equation with respect to m , i.e.

$$\left(\frac{\pi}{L}m\right)^4 - \frac{\rho\nu^2 I_p\omega^2 - EA}{G\nu^2 I_p}\left(\frac{\pi}{L}m\right)^2 - \frac{\rho A\omega^2}{G\nu^2 I_p} = 0 \tag{62}$$

with four roots of m, namely

$$m_{1,2} = \pm\frac{L}{\pi}\sqrt{\frac{\Pi_1 - \sqrt{\Pi_2}}{2}}, m_{3,4} = \pm\frac{L}{\pi}\sqrt{\frac{\Pi_1 + \sqrt{\Pi_2}}{2}} \tag{63}$$

where $\Pi_1 = \frac{\rho\nu^2 I_p\omega^2 - EA}{G\nu^2 I_p}$ and $\Pi_2 = \Pi_1^2 + \frac{4\rho A\omega^2}{G\nu^2 I_p}$. It is obvious that the wavenumber m should be a nonnegative integer value. Therefore, the two negative roots m_2 and m_4 should be omitted and now only m_1 and m_3 are to be considered. Three situations are needed to be taken into consideration.

(1) If $\Pi_2 < 0$, then both m_1 and m_3 are complex value, so

$$J_s = 0 \tag{64}$$

(2) If $\Pi_2 > 0$ and $\Pi_1 - \sqrt{\Pi_2} < 0$, then m_1 is imaginary and m_3 is positive real, so

$$J_s = \text{floor}\left(\frac{L}{\pi}\sqrt{\frac{\Pi_1 + \sqrt{\Pi_2}}{2}}\right) \tag{65}$$

(3) If $\Pi_2 > 0$ and $\Pi_1 - \sqrt{\Pi_2} > 0$, then both m_1 and m_3 are positive real, thus

$$J_s = \text{floor}\left(\frac{L}{\pi}\sqrt{\frac{\Pi_1 - \sqrt{\Pi_2}}{2}}\right) + \text{floor}\left(\frac{L}{\pi}\sqrt{\frac{\Pi_1 + \sqrt{\Pi_2}}{2}}\right) \tag{66}$$

Therefore, J_0 can be determined by Eq.(59).

3.3. The J_0 count for the Mindlin-Herrmann theory

Similarly, for Mindlin-Herrmann theory, deriving the expressions of the mode count J_s of the element with both ends simply supported is the first step. When simply supported on both ends, we have

$$U(0) = U(L) = F_\psi(0) = F_\psi(L) = 0 \tag{67}$$

We can assume

$$\begin{aligned} U(x) &= \sin\left(\frac{m\pi}{L}x\right) \\ \Psi(x) &= k\cos\left(\frac{m\pi}{L}x\right) \end{aligned} \tag{68}$$

where $m = 0, 1, 2, 3...$

(1) For $m = 0$, we have $U(x) = 0$ and $\Psi(x) = k$, corresponding to one rigid mode, we have

$$J_s = 1 \tag{69}$$

(2) For $m = 1, 2, 3...$, we can substitute Eq.(68) into Eqs.(40) and (41) leading to a fourth polynomial equation with respect to m , i.e.

$$a_2\left(\frac{\pi}{L}m\right)^4 + a_1\left(\frac{\pi}{L}m\right)^2 + a_0 = 0 \tag{70}$$

where

$$\begin{aligned} a_2 &= (2\mu + \lambda)A\mu I_p, \\ a_1 &= (2\mu + \lambda)A\rho I_p\omega^2 + \rho A\omega^2\mu I_p - 4\mu(2\mu + 3\lambda)A^2, \\ a_0 &= -\rho A\omega^2[4(\mu + \lambda)A - \rho I_p\omega^2] \end{aligned}$$

where four roots of m exist, namely

$$m_{1,2} = \pm\frac{L}{\pi}\sqrt{\frac{-a_1 - \sqrt{a_1^2 - 4a_0a_1}}{2a_2}}, m_{3,4} = \pm\frac{L}{\pi}\sqrt{\frac{-a_1 + \sqrt{a_1^2 - 4a_0a_1}}{2a_2}} \tag{71}$$

It is known from the physical sense that the wavenumber m should be a nonnegative integer value. Therefore, the two negative roots m_2 and m_4 should be omitted. However, there are still three situations for roots m_1 and m_3.

(i) If $a_1^2 - 4a_0a_1 < 0$, then both m_1 and m_3 are complex value, we have

$$J_s = 1 \tag{72}$$

(ii) If $a_1^2 - 4a_0a_1 > 0$ and $-a_1 - \sqrt{a_1^2 - 4a_0a_1} < 0$ and $-a_1 + \sqrt{a_1^2 - 4a_0a_1} > 0$, then only m_3 is positive real, so

$$J_s = \text{floor}\left(\frac{L}{\pi}\sqrt{\frac{-a_1 + \sqrt{a_1^2 - 4a_0a_1}}{2a_2}}\right) \tag{73}$$

(iii) If $\Pi_2 > 0$ and $\Pi_1 - \sqrt{\Pi_2} > 0$, then both m_1 and m_3 are positive real, thus

$$J_s = \text{floor}\left(\frac{L}{\pi}\sqrt{\frac{-a_1 - \sqrt{a_1^2 - 4a_0a_1}}{2a_2}}\right) + \text{floor}\left(\frac{L}{\pi}\sqrt{\frac{-a_1 + \sqrt{a_1^2 - 4a_0a_1}}{2a_2}}\right) \tag{74}$$

Finally, the J_0 of a Mindlin-Herrmann can be determined based on Eq. (59).

3.4. Mode shape computation

Once the natural frequencies have been computed by the W-W algorithm, the mode shapes can be solved directly. By taking the entry of the displacement vector corresponding to an appropriate degree of freedom equal to arbitrary assigned values, the displacement vector in the global coordinate system can be obtained. Then the displacement vector in the global coordinate system will be transformed to the local coordinate system. The unknown constant vector can be calculated by using the relationships between the force, displacement and constant vectors. Finally, the mode shapes of the structures corresponding to the natural frequency can be recovered.

4. Results and discussion

The theory described above has been implemented into a Matlab program to compute numerical results. To demonstrate the exactness of the method, Section 4.1 validates the present results with the help of those available in the literature. Section 4.2 illustrates the natural frequencies of a rod element with both ends simply supportted based on different theories. In Section 4.3, we computed the natural frequencies based on different theories under all possible boundary conditions. Then, in Section 4.4, we explore the natural frequencies and mode shapes of a stepped rod. Finally, Section 4.5 shows the application to the free vibration analysis of a pin-jointed frame based on the four rod theories.

4.1. Validation and comparisons

In this section, the DS models developed in this paper are validated against existing results in the literatures. A cylindrical rod based on both the Rayleigh-Bishop and the Mindlin-Herrmann theories is selected for the free vibration analyses. Both ends of the rod are simply supported, i.e., the longitudinal deformation of the rod end is fixed whereas the lateral deformation of the rod end is free. The physical and geometric parameters are

the same as the exact solutions of Refs.[19] and [20], i.e., Young modulus $E = 10^{11}Pa$, mass density $\rho = 8.5\times10^{3}kg/m^{3}$, Poisson ratio $\nu = 0.34$, radius $r = 0.5m$, length $l = 1m$.

The first six natural frequencies computed by both the dynamic stiffness method and those in Refs.[19] and [20] are shown in Table 1. It can be clearly seen from Table 1 that the results computed using the DSM match very well with the exact solutions computed in Refs.[19] and [20]. The difference is mainly due to the insufficient precision of the significant figures adopted in the references. It should be emphasized that the current dynamic stiffness method is capable of obtaining results for all possible BCs without deriving new formulations, which is in an apparent contrast to the Green function method in Refs.[19] and [20].

Table 1. The first sixth natural frequencies of longitudinally vibrating Rayleigh-Bishop and Mindlin-Herrmann under simply-simply supported boundary conditions computed by DSM and exact solutions in terms of a Green function as in Ref.[19] and Ref.[20]

Mode No.	Natural frequency (Hz)			
	Rayleigh-Bishop		Mindlin-Herrmann	
	Ref.[19]	DSM	Ref.[20]	DSM
1	1647	1646.53	1637	1636.57
2	3014	3014.27	2883	2882.76
3	4140	4140.49	3335	3334.6
4	5152	5152.47	3750	3750.42
5	6126	6126.38	3855	3855.4
6	7094	7094.28	4793	4793.14

4.2. Comparisons of the natural frequencies based on different theories

The nth natural frequencies of a classical rod with both ends clamped can be found in Ref.[63] given by

$$\omega_{n_C} = n\pi\sqrt{E/\left(\rho L^2\right)} \tag{75}$$

where $n = 1, 2, 3....$ When both ends of a Rayleigh-Love rod are clamped, combined with the physical meaning of the stiffness, it is known that all elements in the dynamic stiffness matrix of the longitudinal free vibration of the Rayleigh Love rod element should be infinite. Thus, we have $\sin\left(\omega L\sqrt{\frac{\rho A}{EA-\nu^2\rho I_p\omega^2}}\right) = 0$, and therefore, the nth natural frequencies of a Rayleigh-Love rod with both ends clamped can be given by[63]

$$\omega_{n_{RL}} = n\pi\sqrt{\frac{E}{\rho L^2}}\sqrt{\frac{AL^2}{AL^2+\nu^2n^2\pi^2I_p}} \tag{76}$$

It is notable that for the Rayleigh-Love theory, there is a cut off frequency ω_0 for the longitudinal vibration of rod element, shown in Fig.2. It means that with the increase of the order of natural frequency, the natural frequency keeps approaching the cut-off frequency ω_0. This is because when $\omega > \sqrt{EA/(\rho I_p\nu^2)}$, the root of the governing equation is imaginary, and there is no harmonic vibration occuring. Ref.[66] also pointed out this limitation.

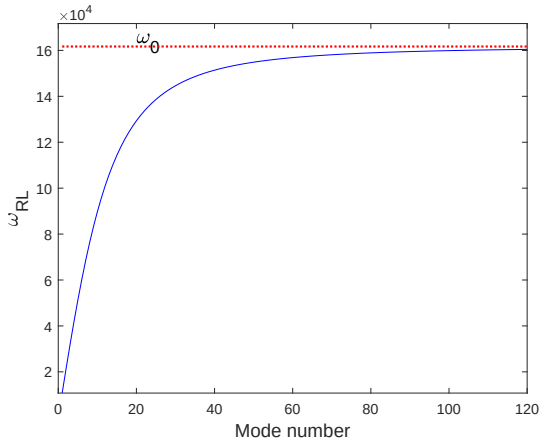

Fig. 2. The cut off frequency of the Rayleigh-Love theory.

Solving the quadratic equation with ω as an independent variable given by Eq.(62) , the nth natural frequencies of a Rayleigh–Bishop rod with both ends simply supported can be given by[19]

$$\omega_{n_{RB}} = n\pi\sqrt{\frac{E}{\rho L^2}}\sqrt{\frac{2(1+\nu)AL^2+\nu^2n^2\pi^2I_p}{2(1+\nu)AL^2+2(1+\nu)\nu^2n^2\pi^2I_p}} \tag{77}$$

Similarly, the natural frequencies of a Mindlin-Herrmann rod with both ends simply supported can be obtained from Eq.(70). The Mindlin-Herrmann theory consists of longitudinal vibration modes and pure transversal vibration modes. The nth natural frequencies correspond to the longitudinal vibration modes can be given by

$$\omega_{n_{MHa}} = \frac{1}{2}n\pi\sqrt{\frac{E}{\rho L^2}}\sqrt{\frac{-8l^2+(-3+4\nu)n^2\pi^2r^2-\sqrt{\left(8l^2-n^2\pi^2r^2\right)^2+128n^2\pi^2\nu^2r^2l^2}}{n^2\pi^2r^2\left(-1+\nu+2\nu^2\right)}} \tag{78}$$

The nth natural frequencies correspond to the pure transversal vibration modes can be given by

$$\omega_{n_{MHt}} = \frac{1}{2}n\pi\sqrt{\frac{E}{\rho L^2}}\sqrt{\frac{-8l^2+(-3+4\nu)n^2\pi^2r^2+\sqrt{\left(8l^2-n^2\pi^2r^2\right)^2+128n^2\pi^2\nu^2r^2l^2}}{n^2\pi^2r^2\left(-1+\nu+2\nu^2\right)}} \tag{79}$$

From above, it follows that the distinction among the four models is dependent on the slenderness ratio L/r as well as the Poisson ratio ν of the material where L is the length of the rod and r is radius of gyration of the cross-section of the rod . The Poisson ratio ν for an isotropic material is generally constant and is assumed to be 0.3 in the following analysis.

Fig.3 illustrates how the natural frequencies of longitudinal vibration vary with slenderness ratio under the boundary condition of simply supported at both ends. As expected, the differences in results for lower values of the slenderness ratios (and higher natural frequencies) are quite pronounced. For instance, compared with the classical the-

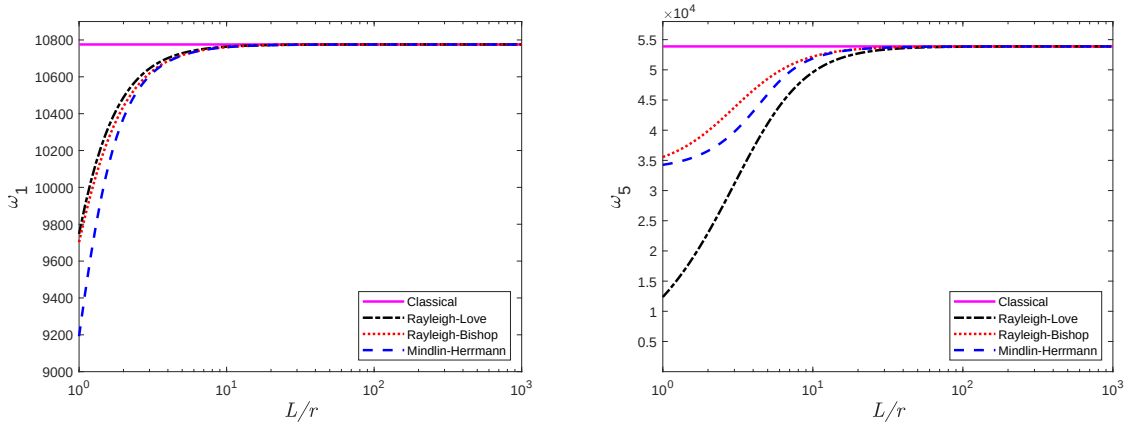

(a) The 1st natural frequency

(b) The 5th natural frequency

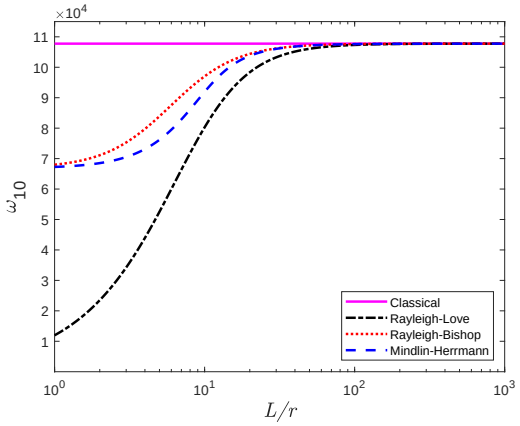

(c) The 10th natural frequency

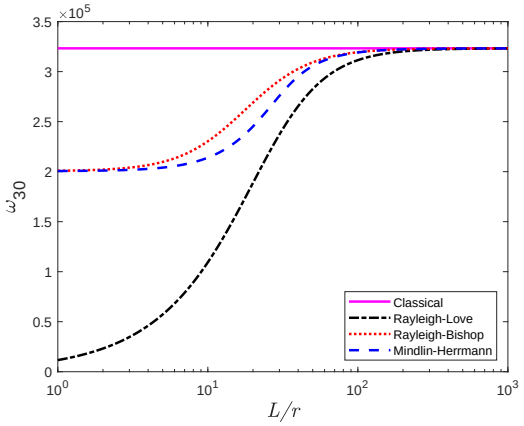

(d) The 30th natural frequency

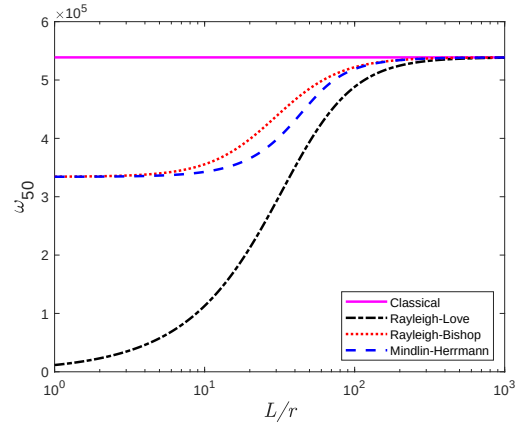

(e) The 50th natural frequency

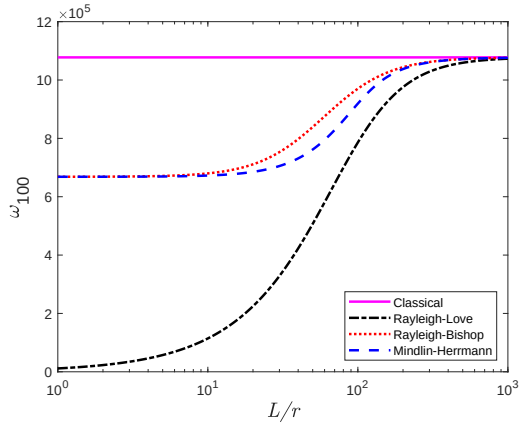

(f) The 100th natural frequency

Fig. 3. Variation of natural frequencies (1st, 5th, 10th, 30th, 50th and 100th) with slenderness ratio(L/r) for the classical, Rayleigh–Love, Rayleigh-Bishop and Mindlin-Herrmann theories under the S-S boundary condition(The abscissa is the logarithmic coordinate).

ory, the discrepancies in the fifth natural frequency for Rayleigh–Love, Rayleigh–Bishop and Mindlin-Herrmann for slenderness ratio 5 are 25%, 10%, 15%, respectively. Therefore, for smaller slenderness ratios and for higher frequency ranges, the lateral deformation of the rod is so important that can not be ignored. Moreover, the Mindlin-Herrmann theory is a more accurate theory for the modal analysis of rod structures within the low, medium and high frequency ranges.

4.3. Comparisions of different boundary conditions

In this section, modal analysis is performed for rods by using the above four theories applying different boundary conditions such as fixed supported, one end fixed, the other end simply supported and simply supported conditions. We consider an isotropic, thick, short rod with a cylindrical section. The material and geometric parameters are as follows: $r = 0.2m, l = 1m, E = 70 \times 10^9 Pa, \nu = 0.3, \rho = 2.7 \times 10^3 kg/m^3$. For the classsical theory and Rayleigh-Love theory, each node has only one longitudinal degree of freedom. So there are three kinds of boundary conditions: fixed-fixed, fixed-free, and free-free. For the Rayleigh-Bishop theory and Mindlin-Herrmann theory, each node has two degrees of freedom with the longitudinal displacement and the cross section rotation. So there are altogether 10 boundary conditions in the combinations of fixed, simply supported, sliding and free.

The natural frequencies using the four rod theories under different boundry conditions computed by DSM are shown in Tables 2 and 3. It should be noted that the letters 'C', 'G', 'S' and 'F' in this section represent 'clamped', 'guided', 'simply-supported' and 'free' boundary conditions, respectively. 'BCs' is an abbreviation for boundary conditions. 'C', 'R-L', 'R-B', 'M-H' represent the classical, Rayleigh-Love, Rayleigh-Bishop, Mindlin-Herrmann theories respectively. In general, the results computed by the dynamic stiffness method can be used as benchmark solutions to assess the results of other approximate methods.

4.4. Application to rod assemblies

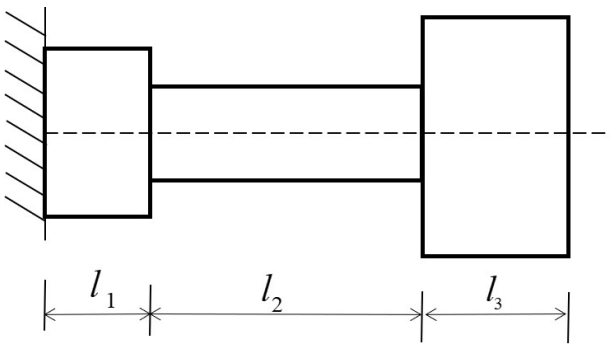

Fig. 4. A three-stepped rod for free vibration analysis.

In this section, the dynamic stiffness method is used to analyze the vibration characteristics of a stepped rod with solid circular cross-section. To get the the global dynamic stiffness matrix of the final structure, we used an assembly process just like that of the finite element method. The specific process is given in the appendix B. As shown in Fig.4,

Table 2. Exact natural frequencies within the low(1st, 3rd and 5th modes), mid(10th, 20th, 30th and 50th modes) and high(100th mode) frequency ranges for a rod subject to 3 different combinations of end constrains based on classical(C), Rayleigh-Love(R-L), Rayleigh-Bishop(R-B), Mindlin-Herrmann(M-H) theories.

BCs	Theory	Natural frequency (Hz)							
		1	3	5	10	20	30	50	100
C-C	C	2545.88	7637.62	12729.4	25458.7	50917.5	76376.3	127294	254587
	R-L	2523.56	7091.7	10592.6	15278.7	17883.8	18530.1	18889.3	19047.2
	R-B	2671.7	7687.3	12013.4	20637.9	35680.6	50825.5	81729.1	160091
	M-H	2603.52	7462.88	11029.8	13526.7	22311.7	32692.6	52838.5	103602
C-F	C	1272.94	6364.69	11456.4	24185.8	49644.6	75103.3	126021	253314
	R-L	1270.12	6038.29	9824.72	14989.9	17826.8	18511.5	18885.1	19046.7
	R-B	1305.42	6317.19	10686.7	19060.9	33662.6	48671.5	79472.6	157770
	M-H	1288.4	6199.24	9842.96	12970.9	21570.3	31706.2	51994.3	102237
F-F	C	0	5091.75	10183.5	22912.9	48371.7	73830.4	124748	252042
	R-L	0	4919.94	8986.14	14671.5	17765.9	18492	18880.7	19046.2
	R-B	0	4979.42	9406.48	17684.5	31698.4	46539.2	77222.9	155451
	M-H	0	4953.47	8841.41	12285.4	20827.5	30381.7	50675.9	101447

the rod structure is composed of three sections, each of which is constructed of different materials and has different cross-sectional areas. The left end of the stepped rod is fully fixed, and the right end is free. The parameters required for dynamic stiffness analysis are as follows:

$r_1 = 0.05m, r_2 = 0.03m, r_3 = 0.075m$

$l_1 = 0.05m, l_2 = 0.17m, l_3 = 0.13m$

$E_1 = 200 \times 10^9 Pa, E_2 = 70 \times 10^9 Pa, E_3 = 100 \times 10^9 Pa$

$\rho_1 = 7.85 \times 10^3 kg/m^3, \rho_2 = 2.7 \times 10^3 kg/m^3, \rho_3 = 8.4 \times 10^3 kg/m^3$

$\nu_1 = 0.30, \nu_2 = 0.33, \nu_3 = 0.34$

The natural frequencies obtained using DSM based on the four theories are shown in Table 4. Due to the existence of the cut-off frequency of Rayleigh love theory, the natural frequencies of the tenth order and higher are not possible to compute. Although, for the first natural frquency, the Mindlin-Herrmann theory is larger than the classical theory (the differences are still well within 1.2%), but for high-order natural frequencies, the Mindlin-Herrmann theory is much smaller and more accurate than other theories.

Table 5 illustrates the 1st, 3rd, 10th, 30th, and 50th mode shapes based on four theories. It can be clearly seen that for the classical and Rayleigh-Love theories, there is only longitudinal deformation, but for the Rayleigh-Bishop and Mindlin-Herrmann theories, the lateral deformation is apparent and cannot be ignored.

4.5. Application to pin-jointed plane frame structures

The higher-order rod theory can be incorporated into pin-jointed frame structures for more accurate results. Fig.5 gives an illustrative example. Each element of the frame has the same uniform geometrical, cross sectional and material properties. Flexural rigidity

Table 3. Exact natural frequencies within the low(1st, 3rd and 5th modes), mid(10th, 20th, 30th and 50th modes) and high(100th mode) frequency ranges for a rod subject to 7 different combinations of end constrains based on Rayleigh-Bishop(R-B) and Mindlin-Herrmann(M-H) theories

BCs	Theory	Natural frequency (Hz)							
		1	3	5	10	20	30	50	100
C-S	R-B	2600.06	7492.03	11731.1	20223.6	35113.5	50184.2	81025.2	159343
	M-H	2567.08	7338.58	10948.8	13501.1	22096.8	32044.7	52090.4	103599
C-G	R-B	1305.49	6325.16	10733.7	19449.2	34369.5	49422.9	80247.9	158556
	M-H	1288.52	6225.55	10185.8	13523.9	22311.3	31844.7	52147.1	103021
S-S	R-B	2532.17	7306.5	11461.7	19822.8	34553.9	49546.9	80322.9	158594
	M-H	2531.73	7219.9	10859.2	13233.5	22044.9	31290.5	51312.3	103020
S-G	R-B	1271.20	6165.87	10482.4	19059.3	33815.4	48788.4	79546.5	157808
	M-H	1271.19	6128.24	10048.8	13077.9	21597.2	31827.6	52090.0	102234
S-F	R-B	1271.15	6158.73	10440.4	18699.3	33116.5	48040.2	78772.2	157022
	M-H	1271.08	6104.26	9729.03	12698.6	20937.7	31281.5	51310.7	102132
G-G	R-B	0	4986.72	9464.61	33078.1	33078.1	48030.6	78770.4	157022
	M-H	0	4973.7	9179.27	22044.9	22044.9	31290.5	51312.3	103020
G-F	R-B	0	4983.06	9435.21	17968.2	32383.9	47283.9	77996.4	156236
	M-H	0	4963.50	8989.75	21570.3	21570.3	30567.9	50697.5	102233

Table 4. Exact natural frequencies covering low-(1st-5th modes), mid-(10th-50th modes) and high-(100th mode) frequency range of a stepped rod in longitudinal vibration using four theories, namely, Classical(C), Rayleigh-Love(R-L), Rayleigh-Bishop(R-B) and Mindlin-Herrmann(M-H).

Mode No.	Natural frequency (Hz)			
	C	R-L	R-B	M-H
1	1184.39	1184.31	165.181	1198.20
2	12509.4	11732.9	12428.2	11677.2
3	15002.6	14503.4	15641.6	14842.5
4	24187.3	20014.4	21570.1	18403.7
5	26578.8	23268.4	27558.9	21923.8
10	59541.9	28865.4	45209.5	36163.3
30	181371	30341.0	121635	87117.2
50	305332	30417.7	196030	132447
100	613992	30446.1	381754	254677

$EI = 4 \times 10^6 Nm^2$, axial rigidity $EA = 8 \times 10^8 N$, mass per unit $\rho A = 30 kg/m$, Poisson ratio $\nu = 0.3$.

By applying the proposed DS formulations of the four rod theories, a wide frequency range of natural frequencies of the frame structure are obtained through both DSM and FEM. Some selected frequencies computed by DSM based on four different theories are compared with FE solutions computed by ANSYS in Table 6. The computation of both DSM and FEM results was performed on the same PC equipped with a 2.40 GHz Intel

Table 5. Mode shapes of a stepped rod in longitudinal vibration based on four different theories, namely, classical(C), Rayleigh-Love(R-L), Rayleigh-Bishop(R-B), Mindlin-Herrmann(M-H), respectively

Mode No.	Mode shapes			
	Classical	Rayleigh-Love	Rayleigh-Bishop	Mindlin-Herrmann
1	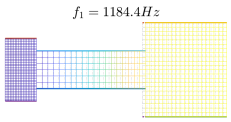	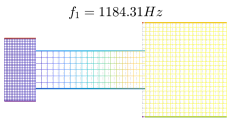	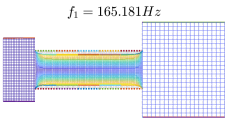	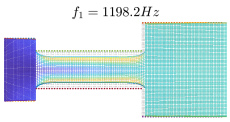
3	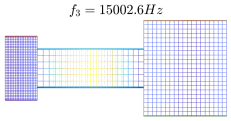	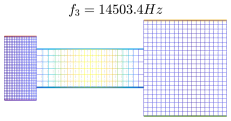	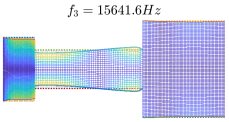	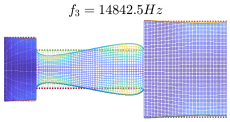
10	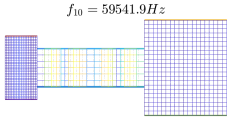	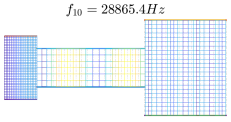	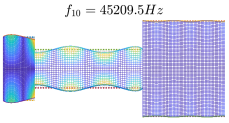	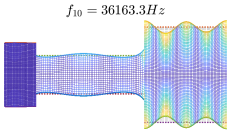
30	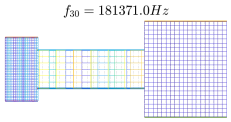	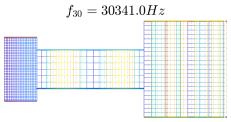	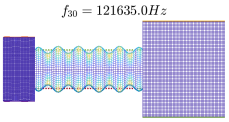	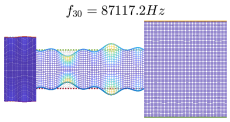
50	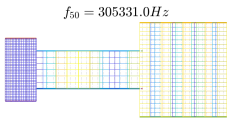	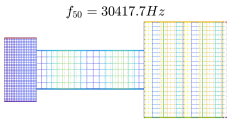	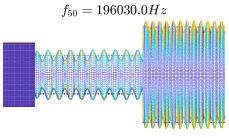	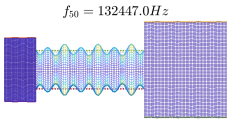

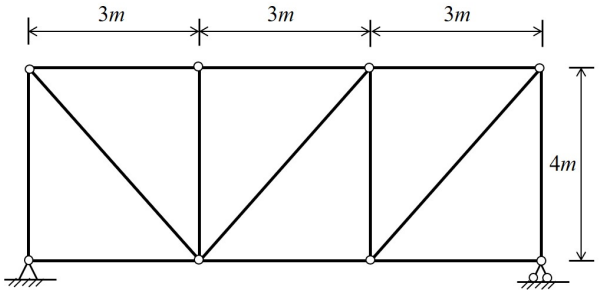

Fig. 5. A pin-jointed plane frame.

Table 6. Natural frequencies in Hz and computational time(Comp. Time) of the pin-jointed plane frame of Fig. 4 using the finite element method(FEM) by using different numbers of elements(N) and by the dynamic stiffness method(DSM) based on four rod theories, namely, classical(C), Rayleigh-Love(R-L), Rayleigh-Bishop(R-B), Mindlin-Herrmann(M-H), respectively. ITC (Impossible To Compute), % Error in FEM relative to R-B shown in the parenthesis.

Mode No.	FEM					DSM			
	N = 13	N = 26	N = 65	N = 780	N = 1300	C	R-L	R-B	M-H
1	48.8655 (-33.16%)	62.5114 (-14.49%)	67.8912 (-7.08%)	72.2833 (-1.06%)	72.4453 (-0.84%)	72.6877	72.6874	73.0610	72.8763
3	122.614 (-19.97%)	132.813 (-13.32%)	143.931 (-6.00%)	151.622 (-0.98%)	151.933 (-0.78%)	152.403	152.401	153.126	152.768
5	187.415 (-30.10%)	228.456 (-14.79%)	255.146 (-4.78%)	265.687 (-0.85%)	266.048 (-0.71%)	266.593	266.581	267.952	267.276
25	(ITC)	1365.09 (-5.16%)	1280.20 (-1.34%)	1285.20 (-0.95%)	1287.39 (-0.78%)	1290.99	1289.56	1297.54	1293.89
50	(ITC)	(ITC)	2994.94 (12.53%)	2643.82 (-0.67%)	2646.84 (-0.55%)	2654.67	2642.30	2661.54	2654.20
100	(ITC)	(ITC)	4367.50 (-16.18%)	5264.03 (1.02%)	5242.20 (0.61%)	5238.84	5145.61	5210.65	5192.44
200	(ITC)	(ITC)	(ITC)	10778.4 6.33%	10593.8 (4.51%)	10505.2	9808.75	10137.1	10012.1
350	(ITC)	(ITC)	(ITC)	20010.7 (20.43%)	18956.4 (14.09%)	18378.9	15262.5	16615.4	15674.6
500	(ITC)	(ITC)	(ITC)	30323.7 (36.91%)	27954.0 (26.22%)	26327.8	18982.9	22147.9	16969.5
Comp. Time(s)	\	\	\	92.56	130.31	6.42	7.934	9.88	12.96

core i7-5500U CPU processor and 8 GB of memory. When using the DSM, only one element for each member is used in the modelling and all DSM results are given with accuracy of six significant figures. The FEM results are computed by using different numbers of elements. When the numbers of elements are not enough in the FEM, the results are unreliable and higher natural modes are not possible to compute. It is apparent that DSM is far more superior to the FEM in free vibration analysis within medium to high frequency ranges. It should be noted that the relative errors between two methods increase at higher modes. There may be two reasons. On one hand, it is because the numbers of elements used in FEM are not enough at high frequency range (Compared with the classical theory, the relative errors of the 500th mode between DSM and FEM is 6.18%). On the other hand, it reflects that the influence of the lateral deformation of the rod structure is apparent and cannot be ignored when analyzing the high-frequency vibration of the rod structures. The major advantage of the proposed DSM lies in the

fact that the DS formulation satisfies the governing differential equation exactly and uses extremely low degree of freedom to represent the system most accurately. Furthermore, it can be seen from Table 6 that when the structure is divided into 1300 elements in FEM, the FEM takes as long as $130s$ to compute the first 500 modes while the DSM only costs $13s$. It is apparent that the DSM gives exact results covering low to high frequency ranges with much higher efficiency than the FEM.

5. Conclusion

In this paper, closed-form dynamic stiffness (DS) formulations for the Rayleigh–Bishop and Mindlin-Herrmann theoris are developed for the first time, which is applicable to the exact vibration analysis of low aspect ratio rods especially within mid to high frequency ranges. First, the general solutions of the governing differential equations of motion based on the classical, Rayleigh-Love, Rayleigh-Bishop and Mindlin-Herrmann rod theories are obtained. Then those general solutions are used as exact shape functions to be substituded into the generalised displacement and force boundary conditions, leading to ensuing analytical DS matrices for different rod elements. As a well-established solution technique, the Wittrick-Williams algorithm is applied for exact modal analysis of individual rod as well as their assemblies. Besides, the difficulty generally encountered in computing the problematic J_0 count when applying the Wittrick-Williams algorithm for modal analysis has been overcome in an elegant and efficient manner.

To verify the accuracy of the developed dynamic stiffness models, the natural frequencies of a cylindrical rod with specific boundary conditions based on the Rayleigh-Bishop and Mindlin-Herrmann theories are provided and validated against existing exact solutions. Comparisons on the natural frequencies made for different theories are also made. The results show that the distinction between the models quickly decreases with the increase of slenderness ratio(L/r) and the decrease of Poisson ratio. Then, the proposed dynamic stiffness matrices are subsequently used for free vibration analysis of a uniform rod under all possible combinations of boundary conditions. The current rod DS formulations has been applied to both cantilevered stepped rods and pin-jointed plane frames to demostrate the wide applicability of the model to complex built-up structures and the high efficiency of the dynamic stiffness method. The theories developed are particularly helpful when analysing mid to high-frequency free vibration of built-up structures. Furthermore, the developed models can be used for the exact free vibration analysis of space frames and multibody systems. The theory developed will be particularly useful when applying statistical energy analysis method for which the modal density is usually very high in the high frequency range.

Acknowledgements

The authors appreciate the supports from National Natural Science Foundation (Grant Nos. 11802345), State Key Laboratory of High Performance Complex Manufacturing (Grant No. ZZYJKT2019-07), Initial Funding of Specially-appointed Professorship (Grant No. 502045001) which made this research possible.

Appendix A. Dynamic stiffness formulation for the Mindlin-Herrmann theory with rectangular section

The governing differential equation (GDE) in the time domain for a rod with rectangular section based on the Mindlin-Herrmann theory can be expressed in the following form[65]

$$(2\mu+\lambda)A\frac{\partial^2 u}{\partial x^2}+\lambda A\frac{\partial \psi}{\partial x}=\rho A\frac{\partial^2 u}{\partial t^2} \tag{A.1}$$

$$\mu I K_1\frac{\partial^2 \psi}{\partial x^2}-(2\mu+\lambda)A\psi-\lambda A\frac{\partial u}{\partial x}=\rho I K_2\frac{\partial^2 \psi}{\partial t^2} \tag{A.2}$$

where $K_1=\frac{12}{\pi^2}, K_2=K_1\left(\frac{1+v}{0.87+1.12v}\right)^2$, I is the moment of inertia of the section. The natural boundary conditions are as follows

$$f_u=(2\mu+\lambda)A\frac{\mathrm{d}u}{dx}+\lambda A\psi \tag{A.3a}$$

$$f_\psi=\mu I K_1\frac{\mathrm{d}\psi}{dx} \tag{A.3b}$$

Assuming that both the lateral and the longitudinal displacements undergo a simple harmonic vibration with an angular frequency of ω over time t, that is

$$u(x,t)=U(x)\sin(\omega t) \tag{A.4a}$$

$$\psi(x,t)=\Psi(x)\sin(\omega t) \tag{A.4b}$$

where $U(x)$ and $\Psi(x)$ are the amplitudes of longitudinal and lateral vibrations, respectively. Substituting Eqs.(A.4a)(A.4b) into Eqs.(A.1) and (A.2) gives

$$\begin{bmatrix}(2\mu+\lambda)A\mathrm{d}^2+\rho A\omega^2 & \lambda A\mathrm{d}\\ \lambda A\mathrm{d} & -\mu I\mathrm{d}^2+4(\mu+\lambda)A-\rho I_p\omega^2\end{bmatrix}\begin{bmatrix}U\\ \Psi\end{bmatrix}=\begin{bmatrix}0\\0\end{bmatrix} \tag{A.5}$$

where $\mathrm{d}=\frac{\mathrm{d}}{\mathrm{dx}}$. Setting the determinant of the coefficient matrix of Eq.(A.5) equal to zero gives the characteristic equation as

$$a_2k^4-a_1k^2+a_0=0 \tag{A.6}$$

where

$$\begin{aligned}a_2&=(2\mu+\lambda)A\mu I K_1,\\ a_1&=-(2\mu+\lambda)\rho I A K_2\omega^2-\rho A\omega^2\mu I K_1+4\mu(\mu+\lambda)A^2,\\ a_0&=-\rho A\omega^2[(2\mu+\lambda)A-\rho I K_2\omega^2]\end{aligned}$$

The solution of Eq.(A.6) is given by

$$k_i^2=\frac{a_1\pm\sqrt{a_1^2-4a_2a_0}}{2a_2} \tag{A.7}$$

when $i=1$, take '+'; when $i=2$, take '-'. Then the general solution of the rod displacement is

$$U(x)=A_1R_1\sinh k_1x+A_2R_1\cosh k_1x+A_3R_2\sinh k_2x+A_4R_2\cosh k_2x \tag{A.8a}$$

$$\Psi(x)=A_1\cosh k_1x+A_2\sinh k_1x+A_3\cosh k_2x+A_4\sinh k_2x \tag{A.8b}$$

where $R_i = \frac{-k_i\lambda A}{(2\mu+\lambda)Ak_i^2+\rho A\omega^2} = \frac{-k_i\lambda}{(2\mu+\lambda)k_i^2+\rho\omega^2}, i = 1, 2$. Substituting Eq.(A.4) into Eq.(A.3), the expression for the amplitude of the force can be given by

$$F_u = (\lambda + 2\mu) A\frac{\mathrm{d}U}{\mathrm{d}x} + 2\lambda A\Psi \tag{A.9a}$$

$$F_\psi = \mu I K_1 \frac{\mathrm{d}\Psi}{\mathrm{d}x} \tag{A.9b}$$

The boundary conditions for displacements and forces at both ends of the rod can be applied as follows

$$U(0) = U_1, \Psi(0) = \Psi_1, F_u(0) = -F_{u1}, F_\psi(0) = -F_{\psi 1} \tag{A.10a}$$

$$U(L) = U_2, \Psi(L) = \Psi_2, F_u(L) = F_{u2}, F_\psi(L) = F_{\psi 2} \tag{A.10b}$$

Substituting Eq.(A.10) into Eqs.(A.8) and (A.9), the relationships between displacement and constant vectors, force and constant vectors can be derived respectively.

$$\begin{bmatrix} U_1 \\ \Psi_1 \\ U_2 \\ \Psi_2 \end{bmatrix} = \begin{bmatrix} 0 & R_1 & 0 & R_2 \\ 1 & 0 & 1 & 0 \\ R_1Sh_1 & R_1Ch_1 & R_2Sh_2 & R_2Ch_2 \\ Ch_1 & Sh_1 & Ch_2 & Sh_2 \end{bmatrix} \begin{bmatrix} C_1 \\ C_2 \\ C_3 \\ C_4 \end{bmatrix} \tag{A.11}$$

$$\begin{bmatrix} F_{u1} \\ F_{\psi 1} \\ F_{u2} \\ F_{\psi 2} \end{bmatrix} = \begin{bmatrix} -k_1M_1R_1 - M_2 & 0 & (-k_2M_1R_2 - M_2) & 0 \\ 0 & -k_1M_3 & 0 & -k_2M_3 \\ (k_1M_1R_1 + M_2)Ch_1 & (k_1M_1R_1 + M_2)Sh_1 & (k_2M_1R_2 + M_2)Ch_2 & (k_2M_1R_2 + M_2)Sh_2 \\ k_1M_3Sh_1 & k_1M_3Ch_1 & k_2M_3Sh_2 & k_2M_3Ch_2 \end{bmatrix} \begin{bmatrix} C_1 \\ C_2 \\ C_3 \\ C_4 \end{bmatrix} \tag{A.12}$$

where $Ch_1 = \cosh(Lk_1), Sh_1 = \sinh(Lk_1), Ch_2 = \cosh(Lk_2), Sh_2 = \sinh(Lk_2)$ and $M_1 = (2\mu + \lambda) A, M_2 = \lambda A, M_3 = \mu I K_1$.

By eliminating the constant vector from Eqs.(A.11) and (A.12), the DS formulation for the Mindlin-Herrmann theory can be derived as

$$\boldsymbol{f} = \boldsymbol{K}_{MHs}\boldsymbol{d} \tag{A.13}$$

where $\boldsymbol{f} = \begin{bmatrix} F_{u1} & F_{\psi 1} & F_{u2} & F_{\psi 2} \end{bmatrix}^T$ represents the force vector, $\boldsymbol{d} = \begin{bmatrix} U_1 & \Psi_1 & U_2 & \Psi_2 \end{bmatrix}^T$ represents the displacement vector at both ends, $\boldsymbol{K}_{MHs}$ represents the DS matrix of the Mindlin-Herrmann rod with square section, namely

$$\boldsymbol{K}_{MHs} = \begin{bmatrix} G_1 & G_2 & G_4 & G_5 \\ G_2 & G_3 & -G_5 & G_6 \\ G_4 & -G_5 & G_1 & -G_2 \\ G_5 & G_6 & -G_2 & G_3 \end{bmatrix} \tag{A.14}$$

where

$$
\begin{aligned}
G_1 &= M_1\left(-R_2Ch_2Sh_1 + R_1Ch_1Sh_2\right)\left(R_1k_1 - R_2k_2\right)/\delta \\
G_2 &= M_3\left[R_1\left(-Sh_1Sh_2k_1 - k_2 + Ch_1Ch_2k_2\right) + R_2\left(-k_1 + Ch_1Ch_2k_2 - Sh_1Sh_2k_2\right)\right]/\delta \\
G_3 &= M_3\left(-R_1Ch_2Sh_1 + R_2Ch_1Sh_2\right)\left(R_2k_1 - R_1k_2\right)/\delta \\
G_4 &= -M_1\left(-R_2Sh_1 + R_1Sh_2\right)\left(R_1k_1 - R_2k_2\right)/\delta \\
G_5 &= -M_1R_1R_2\left(Ch_1 - Ch_2\right)\left(R_1k_1 - R_2k_2\right)/\delta \\
G_6 &= -M_3\left(-R_1Sh_1 + R_2Sh_2\right)\left(R_2k_1 - R_1k_2\right)/\delta \\
\delta &= 2R_1R_2\left(1 - Ch_1Ch_2\right) + \left(R_1^2 + R_2^2\right)Sh_1Sh_2
\end{aligned}
\tag{A.15}
$$

References

[1] Q. Wang, V. K. Varadan, Longitudinal wave propagation in piezoelectric coupled rods, Smart Materials and Structures 11 (1) (2002) 48–54. doi:10.1088/0964-1726/11/1/305.

[2] L. Li, Y. Guo, Analysis of longitudinal waves in rod-type piezoelectric phononic crystals, Crystals 6 (4) (2016). doi:10.3390/cryst6040045.

[3] F. Cannizzaro, J. De Los Rios, S. Caddemi, I. Caliò, S. Ilanko, Crack localization in beams by frequency shifts due to roving mass with rotary inertia, Procedia Engineering 199 (2017) 900–905. doi:10.1016/j.proeng.2017.09.229.

[4] M. K. Kalkowski, J. M. Muggleton, E. Rustighi, An experimental approach for the determination of axial and flexural wavenumbers in circular exponentially tapered bars, Journal of Sound and Vibration 390 (2017) 67–85. doi:10.1016/j.jsv.2016.10.018.

[5] J. D. Achenbach, Wave Propagation in Elastic Solids, North-Holland Series in Applied Mathematics and Mechanics, Elsevier, Amsterdam, 1975.

[6] J. Rayleigh, R. B. Lindsay, The theory of sound, Dover Publications, 1945.

[7] A. E. H. Love, A treatise on the mathematical theory of elasticity, Dover Publications (2011).

[8] R. E. D. Bishop, Longitudinal Waves in Beams, Aeronautical Quarterly 3 (4) (1952) 280–293.

[9] R. D. Mindlin, G. Herrmann, A one dimensional theory of compressional wave in an elastic rod, in: Proceedings of First US National Congress of Applied Mechanics, Anaheim, 1950, pp. 187–191.

[10] V. V. Zozulya, A higher order theory for shells, plates and rods, International Journal of Mechanical Sciences 103 (2015) 40–54. doi:10.1016/j.ijmecsci.2015.08.025.

[11] J. B. Han, S. Y. Hong, J. H. Song, H. W. Kwon, Vibrational energy flow models for the Rayleigh-Love and Rayleigh-Bishop rods, Journal of Sound and Vibration 333 (2) (2014) 520–540.

[12] M. Machado, J. Dos Santos, Effect and identification of parametric distributed uncertainties in longitudinal wave propagation, Applied Mathematical Modelling 98 (2021) 498–517. doi:https://doi.org/10.1016/j.apm.2021.05.018.

[13] M. Krawczuk, J. Grabowska, M. Palacz, Longitudinal wave propagation. Part I-Comparison of rod theories, Journal of Sound and Vibration 295 (3-5) (2006) 461–478. doi:10.1016/j.jsv.2005.12.048.

[14] M. Krawczuk, J. Grabowska, M. Palacz, Longitudinal wave propagation. Part II-Analysis of crack influence, Journal of Sound and Vibration 295 (3-5) (2006) 479–490. doi:10.1016/j.jsv.2005.12.049.

[15] C. Mei, Comparison of the four rod theories of longitudinally vibrating rods, JVC/Journal of Vibration and Control 21 (8) (2015) 1639–1656.

[16] K. Yang, A unified solution for longitudinal wave propagation in an elastic rod, Journal of Sound and Vibration 314 (1-2) (2008) 307–329.

[17] J. Marais, I. Fedotov, M. Shatalov, Longitudinal vibrations of a cylindrical rod based on the Rayleigh-Bishop theory, Afrika Matematika 26 (7-8) (2015) 1549–1560. doi:10.1007/s13370-014-0286-3.

[18] Y. Gai, I. Fedotov, M. Shatlov, Analysis of a raylegih-bishop model for a thick bar, Proceedings - IEEE Ultrasonics Symposium 1 (2006) 1915–1917. doi:10.1109/ULTSYM.2006.481.

[19] I. A. Fedotov, A. D. Polyanin, M. Y. Shatalov, H. M. Tenkam, Longitudinal vibrations of a Rayleigh-Bishop rod, Doklady Physics 55 (12) (2010) 609–614. doi:10.1134/S1028335810120062.

[20] H. M. Tenkam, R. Anguelov, I. Fedotov, M. Shatalov, Exact solution of the Mindlin–Herrmann model for longitudinal vibration of an isotropic rod, Journal of Engineering Mathematics 99 (1) (2016) 185–201. doi:10.1007/s10665-015-9827-5.

[21] U. Güven, Two mode Mindlin-Herrmann rod solution based on modified couple stress theory, ZAMM Zeitschrift fur Angewandte Mathematik und Mechanik 94 (12) (2014) 1011–1016. doi:10.1002/zamm.201300066.

[22] A. Żak, M. Krawczuk, Assessment of rod behaviour theories used in spectral finite element modelling, Journal of Sound and Vibration 329 (2010) 2099–2113. doi:10.1016/j.jsv.2009.12.019.

[23] L. Xie, S. Wang, J. Ding, R. Banerjee, J. Wang, An accurate beam theory and its first-order approximation in free vibration analysis, Journal of Sound and Vibration 485 (2020) 115567. doi:10.1016/j.jsv.2020.115567.

[24] C. Bian, B. Huang, L. Xie, L. Yi, L. Yuan, J. Wang, Propagation of axisymmetric stoneley waves in elastic solids, Acta Physica Polonica A 139 (2021) 124–131. doi:10.12693/APhysPolA.139.124.

[25] H. Chen, R. Wu, L. Xie, J. Du, J. Wang, High-frequency vibrations of circular and annular plates with the mindlin plate theory, Archive of Applied Mechanics 90 (5) (2020).

[26] W. Shen, D. Li, J. Ou, Modeling dispersive waves in cracked rods using the wavelet-based higher-order rod elements, International Journal of Mechanical Sciences 166 (2020) 105236. doi:10.1016/j.ijmecsci.2019.105236.

[27] C. Gan, Y. Wei, S. Yang, Longitudinal wave propagation in a rod with variable cross-section, Journal of Sound and Vibration 333 (2) (2014) 434–445.

[28] C. W. Lim, Z.-Y. Chen, A new static analysis approach for free vibration of beams, International Journal of Applied Mechanics 10 (01 2018). doi:10.1142/S1758825118500047.

[29] F. Lin, H.-S. Shen, C. W. Lim, Y. Xiang, Assessment of first and third order shear deformation beam theories for the buckling and vibration analysis of nanobeams incorporating surface stress effects, International Journal of Mechanical Sciences 186 (2020) 105873. doi:10.1016/j.ijmecsci.2020.105873.

[30] H. Zhang, J. Ma, H. Ding, L. Chen, Vibration of axially moving beam supported by viscoelastic foundation, Applied Mathematics and Mechanics (2017).

[31] Y. B. Wang, H. Ding, L. Q. Chen, Vibration of axially moving hyperelastic beam with finite deformation, Applied Mathematical Modelling 71 (JUL.) (2019) 269–285.

[32] D. B. Zhang, Y. Q. Tang, R. Q. Liang, L. Yang, L. Q. Chen, Dynamic stability of an axially transporting beam with two-frequency parametric excitation and internal resonance, European Journal of Mechanics / A Solids 85 (2020) 104084. doi:10.1016/j.euromechsol.2020.104084.

[33] W. Yan, C. W. Lim, W. Q. Chen, J. B. Cai, Modeling of EMI response of damaged Mindlin-Herrmann rod, International Journal of Mechanical Sciences 49 (12) (2007) 1355–1365. doi:10.1016/j.ijmecsci.2007.04.007.

[34] H. Sun, Z. Wang, J. Nie, Y. Zhang, R. Xiao, Generalized finite difference method for a class of multidimensional space-fractional diffusion equations, Computational Mechanics 67 (2021) 1–16. doi:10.1007/s00466-020-01917-y.

[35] D. Q. Cao, D. Liu, H. T. Wang, Nonlinear dynamic modelling for mems components via the cosserat rod element approach, Journal of Micromechanics and Microengineering 15 (6) (2005) 1334–1343(10).

[36] D. Q. Cao, D. Liu, H.-T. Wang, Three-dimensional nonlinear dynamics of slender structures: Cosserat rod element approach, International Journal of Solids and Structures 43 (3) (2006) 760–783. doi:https://doi.org/10.1016/j.ijsolstr.2005.03.059.

[37] D. Q. Cao, M. Song, R. Tucker, W. Zhu, D. Liu, W. Huang, Dynamic equations of thermoelastic cosserat rods, Communications in Nonlinear Science and Numerical Simulation 18 (7) (2013) 1880–1887. doi:https://doi.org/10.1016/j.cnsns.2012.11.011.

[38] L. Dai, R. Xiao, Optimal design and analysis of deployable antenna truss structure based on dynamic characteristics restraints, Aerospace Science and Technology 106 (2020) 106086. doi:10.1016/j.ast.2020.106086.

[39] V. Koloušek, Anwendung des Gesetzes der virtuellen Verschiebungen und des Reziprozitätssatzes in der Stabwerksdynamik, Ingenieur-Archiv 12 (6) (1941) 363–370.

[40] F. Han, D. Dan, W. Cheng, J. Zang, A novel analysis method for damping characteristic of a type of double-beam systems with viscoelastic layer, Applied Mathematical Modelling 80 (2020) 911–928.

doi:https://doi.org/10.1016/j.apm.2019.11.008.

[41] H. Han, L. Liu, D. Cao, Analytical approach to coupled bending-torsional vibrations of cracked Timoshenko beam, International Journal of Mechanical Sciences 166 (2020) 105235. doi:10.1016/j.ijmecsci.2019.105235.

[42] A. Burlon, G. Failla, F. Arena, Exact frequency response of two-node coupled bending-torsional beam element with attachments, Applied Mathematical Modelling 63 (2018) 508–537. doi:https://doi.org/10.1016/j.apm.2018.06.047.

[43] J. R. Banerjee, Review of the dynamic stiffness method for free-vibration analysis of beams, Transportation Safety and Environment 1 (2) (2019) 106–116. doi:10.1093/tse/tdz005.

[44] J. R. Banerjee, A. Ananthapuvirajah, X. Liu, C. Sun, Coupled axial-bending dynamic stiffness matrix and its applications for a Timoshenko beam with mass and elastic axes eccentricity, Thin-Walled Structures 159 (August) (2021) 107197.

[45] X. Liu, X. Zhao, C. Xie, Exact free vibration analysis for membrane assemblies with general classical boundary conditions, Journal of Sound and Vibration 485 (2020) 115484. doi:10.1016/j.jsv.2020.115484.

[46] T. Kim, U. Lee, Exact spectral element model for rectangular membranes subjected to transverse vibrations, International Journal of Mechanical Sciences 165 (JAN 2020). doi:{10.1016/j.ijmecsci.2019.105191}.

[47] X. Liu, X. Liu, S. Xie, A highly accurate analytical spectral flexibility formulation for buckling and wrinkling of orthotropic rectangular plates, International Journal of Mechanical Sciences 168 (March) (2020) 105311. doi:10.1016/j.ijmecsci.2019.105311.

[48] H. Li, X. Yin, W. Wu, Dynamic stiffness formulation for in-plane and bending vibrations of plates with two opposite edges simply supported, Journal of Vibration and Control 24 (9) (2018) 1652–1669. doi:10.1177/1077546316667205.

[49] X. Liu, X. Liu, W. Zhou, An analytical spectral stiffness method for buckling of rectangular plates on winkler foundation subject to general boundary conditions, Applied Mathematical Modelling 86 (2020) 36–53. doi:https://doi.org/10.1016/j.apm.2020.05.010.

[50] N. Nanda, Wave propagation analysis of laminated composite shell panels using a frequency domain spectral finite element model, Applied Mathematical Modelling 89 (2021) 1025–1040. doi:https://doi.org/10.1016/j.apm.2020.07.006.

[51] T. I. Thinh, M. C. Nguyen, Dynamic stiffness method for free vibration of composite cylindrical shells containing fluid, Applied Mathematical Modelling 40 (21) (2016) 9286–9301. doi:https://doi.org/10.1016/j.apm.2016.06.015.

[52] B. Zhenning, W. L. Vincent, L. Jianwen, Y. Yang, Dynamic 2.5d green's functions for moving distributed loads acting on an inclined line in a multi-layered ti half-space, Soil Dynamics and Earthquake Engineering 99 (2017) 172–188. doi:https://doi.org/10.1016/j.soildyn.2017.05.003.

[53] Y. H. Chen, Axially-loaded damped Timoshenko beam on viscoelastic foundation, International Journal for Numerical Methods in Engineering 36 (September 1991) (1993) 1013–1027.

[54] Y. H. Chen, J.-T. Sheu, Beam length and dynamic stiffness, Computer methods in applied mechanics and engineering 7825 (95) (1995) 0–7.

[55] M. Ling, A general two-port dynamic stiffness model and static/dynamic comparison for three bridge-type flexure displacement amplifiers, Mechanical Systems and Signal Processing 119 (2019) 486–500. doi:https://doi.org/10.1016/j.ymssp.2018.10.007.

[56] J. F. Doyle, Wave Propagation in Structures, Springer-Verlag, 1989.

[57] S. R. Wu, Classical solutions of forced vibration of rectangular plate driven by displacement boundary conditions, Journal of Sound and Vibration 291 (3-5) (2006) 1104–1121.

[58] H. Ding, M. Zhu, L. Chen, Dynamic stiffness method for free vibration of an axially moving beam with generalized boundary conditions, Applied Mathematics and Mechanics (2019).

[59] A. N. Bercin, An assessment of the effects of in-plane vibrations on the energy flow between coupled plates, Journal of Sound and Vibration 191 (5) (1996) 661–680.

[60] Z. Ba, M. Wu, J. Liang, 3d dynamic responses of a multi-layered transversely isotropic saturated half-space under concentrated forces and pore pressure, Applied Mathematical Modelling 80 (2020) 859–878. doi:https://doi.org/10.1016/j.apm.2019.11.014.

[61] F. W. Williams, W. H. Wittrick, An automatic computational procedure for calculating natural frequencies of skeletal structures, International Journal of Mechanical Sciences 12 (9) (1970) 781–791. doi:10.1016/0020-7403(70)90053-6.

[62] W. H. Wittrick, F. W. Williams, A general algorithm for computing natural frequencies of elastic structures, Journal of Mechanics and applied mathematics XXIV (September 1970) (1971).

[63] J. R. Banerjee, A. Ananthapuvirajah, An exact dynamic stiffness matrix for a beam incorporating Rayleigh–Love and Timoshenko theories, International Journal of Mechanical Sciences 150 (October 2018) (2019) 337–347. doi:10.1016/j.ijmecsci.2018.10.012.

[64] I. Fedotov, M. Shatalov, J. Marais, Hyperbolic and pseudo-hyperbolic equations in the theory of vibration, Acta Mechanica 227 (11) (2016) 3315–3324. doi:10.1007/s00707-015-1537-6.

[65] K. F. Graff, Wave Motion in Elastic Solid, Dover Publications, 1991.

[66] M. Predoi, C. Petre, O. Vasile, M. Boiangiu, High frequency longitudinal damped vibrations of a cylindrical ultrasonic transducer, Shock and Vibration 2014 (2014) 1–8. doi:10.1155/2014/105971.